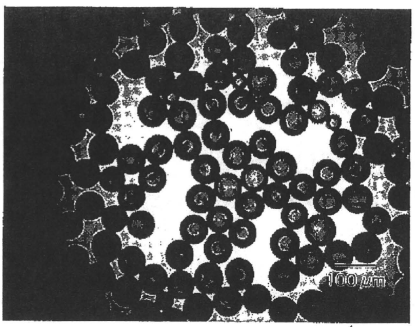

第1図　マイクロカプセルF-80Eの顕微鏡写真

ズを用いるべきであるが、後述する模擬血管の製作限界に対する顕微鏡の倍率との関係上、この範囲となった。カプセルの顕微鏡写真を第1図に示す。

マイクロスフェアーは粉体状で存在し、そのサイズは30 μm以下のものから120 μm程度のものまで含まれる。そこでカプセルを水に溶かし、目開き各38、63、75、90 μmの篩（ふるい）を用いてカプセルサイズを選別した。

2−2　水流中のカプセルに対する音響作用力

マイクロサイズのカプセルやバブルは内部に気体を含むため、超音波照射下で膨張収縮運動（体積振動）を行う。この体積振動とカプセル付近の音圧勾配の積の時間平均によりカプセルが超音波から受ける音響放射力が決まる。一般的に、音響放射力とはカプセルを定在波の腹や節に捕捉する力、進行波によってビーム方向へ移動させる力である。そしてこの力は水流中を流れるマイクロカプセルにも作用し、第2図に示すように超音波の照射方向にカプセルを移動させることが出来ると考えられる。

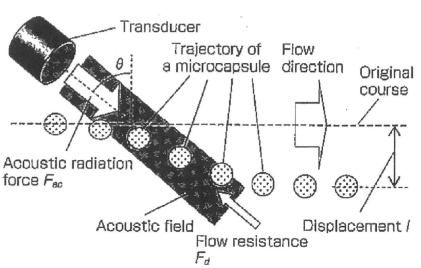

第2図　超音波照射下で流体中に存在するマイクロカプセルの軌跡

音響放射力Facは、式(1)で表される。

$$F_{ac}=\frac{4}{3}\pi R_0^3 A\frac{P_A^2}{\rho c^2} \qquad \cdots(1)$$

ここでρは媒質の密度、cは音速、P_Aは音圧、R_0はカプセル径、Aは定数である。流路内では、カプセルはストークスの法則より得られる水流からの抗力を受けるため、音響放射力の発生方向に、ストークス抵抗に逆らいながら第2図に示すように移動すると考えられる。

2−3　模擬血管とカプセルの挙動観察法

実験に用いる模擬血管として、超音波透過性に優れたポリエチレングリコールを用いて外形80×50×15 mmの直方体を作成し、その内部に第3図のように内径2 mmで1：2のY字型分岐を形成した。分岐部における超音波照射下のカプセル挙動を観察するために、図中のobserved area 1を倒立顕微鏡(DMIRB, LEICA社製）で観測する実験系を構築した。

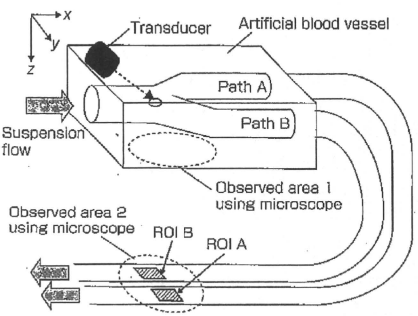

第3図　Y字分岐を有する模擬血管とトランスデューサの配置

この実験系を用いて分岐部を流れるカプセルの挙動を顕微鏡に接続した高速度カメラで観察した。超音波の発生は、ファンクションジェネレータにより発生させた正弦波を高周波増幅器で増幅し、中心周波数1 MHzの集束型超音波トランスデューサから照射した。また65〜73 μmのカプセルの共振周波数は約100 kHz前後であり、これによって超音波照射によるカプセル崩壊の可能性は小さい。また超音波の音圧と水流の流速の範囲は、120〜160 kPa、100〜

250 mm/sとした。

2−4 模擬血管の分岐部に対する超音波照射法

トランスデューサは直径25 mmの円筒形で、照射面から中心軸上45 mmの位置で放射音圧が最大（半値幅約3 mm）となることから、トランスデューサの設置は模擬血管の流路との距離を45 mmに保つことにした。超音波を照射する地点は第4図に示す各地点で、模擬血管の中心軸交点をO地点とし、この点を基準にP、Q、Rを1 mm間隔に決定した。そしてO〜Rの各地点を中心としてトランスデューサをy-z平面に対して50°と固定し、さらにx-y平面上のトランスデューサの設置角度θを−50〜80°まで変化させた。また超音波照射地点の変更は、照射角度を決めた後にx-yステージを用いて行った。

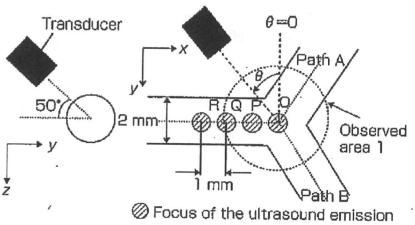

第4図 模擬血管に対する超音波の照射方法

ここで流速100 mm/sで流路を流れる直径65〜73 μmのカプセル懸濁液に対して、音圧160 kPaで周波数1 MHzの正弦波の集束超音波を第4図のQ地点にθ=60°で照射した時のobserved area 1の連続写真を第5図に示す。(a)はカプセル懸濁液を注入直後で、各写真の時間間隔は1 secである。カプセルは流路壁面に押さえつけられ、流路B側に誘導される様子が観察された。この現象は超音波の照射を停止するとほぼ同時に確認されなくなった。そのためカプセル誘導が音響放射力によって起こされたことが確認された。

2−5 流路を流れるカプセル量の評価

前述の実験系で示した分岐部を観察するだけでは、定量的なカプセル量を計測できない。そこで第3図に示した模擬血管の分岐後に外径2 mm，内径1 mmの半透明なチューブを接続して延長し、分岐点の下流300 mmの下流地点をobserved area 2とし、流路が平行になるように配置した。observed area 2の観測画面を第6図に示す。流路A、Bを通過するカプセルの計測法として、第6図に示される撮影範囲内に、同じ大きさの2つの関心領域を設定し、カプセルを流していない状態の画像の関心領域内における輝度平均値と比較した。具体的には、カプセルを流す前の関心領域の輝度平均値をREFとし、カプセルが流れている間の輝度平均値との差を式(2)のように計算し、REFとの比をShadow indexとして次式のように定義した。

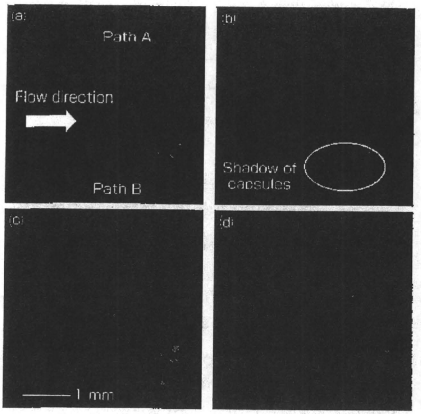

第5図 Observed area 1で観察できるマイクロカプセルの誘導

$$\sigma=\left(REF-\sum_{x}\sum_{y}f(x,y)\right)/REF \qquad \cdots(2)$$

ただし、fは画素の輝度値であり、ROI A、Bそれぞれに Shadow indexを計測した。この値はカプセル懸濁液の濃度と流速に依存するため、条件を固

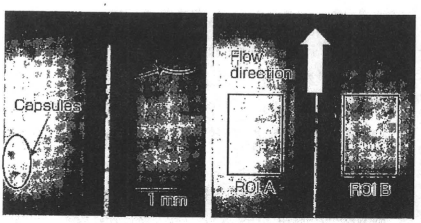

(a) 超音波照射なし　(b) 超音波照射あり

第6図 Observed area 2におけるマイクロカプセル濃度の計測

定する必要があるが、検証の結果、カプセル濃度が0.15～0.25 g/Lの範囲で300 mm/s以下の流速であれば、Shadow indexの変化を顕著に捉えられることが分かった[04]。よって以後の実験は濃度0.2 g/Lのカプセル懸濁液を用いて実験を行った。

3. カプセル誘導実験とその結果

3－1 超音波の照射位置・角度変化に対するカプセル誘導性能

流速100 mm/sで流路を流れるカプセルに対して、周波数1 MHz、音圧160 kPaの超音波を第4図に示す模擬血管の分岐部O～R地点に照射した。超音波の照射位置と角度によって、両流路へ流れるカプセル量に差があることが観測されたため、ROI BのShadow indexからROI AのShadow indexを減算することにより、流路B方向へ誘導されるカプセル量を評価した。その結果を第7図に示す。

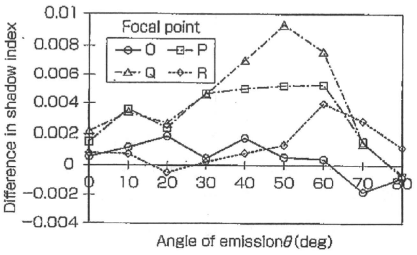

第7図 流路の分岐部への照射超音波の角度とカプセル誘導効率の関係
(流速100 mm/s、周波数1 MHz、音圧160 kPa)

この結果より、最も効率良く分岐部でカプセルを誘導するためには、超音波の焦点をQ、照射角度θ＝50°にした時であった。また焦点を分岐点（O）にすると、どの角度から超音波を照射してもカプセルを誘導することは出来なくなった。また上記の傾向は、超音波の照射を、流路AとBを逆にしても同様であった。これよりカプセル誘導を効率よく行うためには、超音波の照射位置と角度が重要であることが示唆された。

3－2 音圧・流速変化によるカプセル誘導実験

前節にて導出した条件（焦点Q, θ＝50°）を固定し、音圧と流速を変化させてカプセル誘導性能を比較した。第8図に流速を100 mm/sに固定し、音圧を変化させたときの結果を、また第9図に音圧を160 kPaに固定し、流速を変化させたときの結果を示す。両図とも、棒グラフはShadow index値を、折れ線グラフは計算によって求めたカプセル移動距離（第2図）[04]を示す。

この結果より周波数1 MHzの超音波でカプセル誘導を実現するためには、約150 kPa以上の音圧で150 mm/s以下の流速が必要なことが明らかとなった。

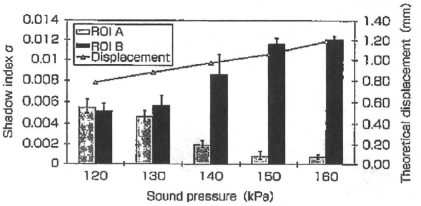

第8図 照射超音波の音圧の変化に対するROI A及びBにおけるShadow index の変化
(周波数1 MHz、流速100 mm/s)

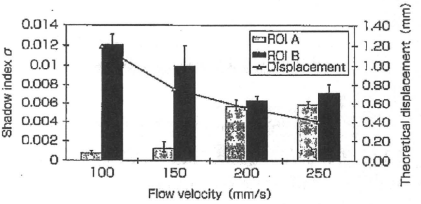

第9図 流速の変化に対するROI A及びBにおけるShadow indexの変化
(周波数1 MHz、焦点音圧160 kPa)

4. 実験結果に対する考察

3－1節の結果より、カプセルを分岐部で誘導するためには、超音波の照射位置と角度が重要な要因であることが示された。そこでカプセル誘導が可能であった時の超音波の音場分布を分岐部に重ねてみると、カプセル誘導が可能となる超音波の照射方法は、誘導する流路と超音波の進行方向が交差する場合であった。このことから流路分岐部でカプセルを誘導するための条件は、分岐前の地点と目的流路の両方の領域を超音波が通過する事と考えられた。

また3－2節の実験より、160 kPa程度の高音圧であればカプセルの誘導が可能であり、音圧を下げるに従いカプセルの誘導精度が落ちていることがわかる。これは音響放射力が小さくなるため、カプセルを目的の流路に移動させることが出来ないためと考えられる。一方、流速が速くなるに従って、カプセルが音場領域を通過する時間が短くなる。そのため、カプセルが受ける音響放射力の影響が小さくなり、カプセルの誘導が起こり難くなると考えられる。

また本研究の実験で使用した最大音圧は160 kPaであるが、この程度であればMI値は0.16程度となり、安全上の問題はない。最後にカプセルのサイズに関しては、今回は63～75 μmを使用したが、生体応用を考えるとこのサイズでは抹消血管を通過できない。音響放射力は式(1)に示すようにカプセルの体積に比例するため、生体内で使用可能な赤血球サイズのカプセルを使用する場合、カプセル径が約1/8になるため、音響放射力は1/500程度になると考えられる。しかしこの技術の最終目標はカテーテルの到達が困難な抹消血管であり、その血流は数mm/sと考えられる。今回は100 mm/s～250 mm/sの範囲の流速を用いたため、カプセルサイズを小さくすることによって音響放射力が低下した場合でも、同様の現象を起こす条件は導出可能と考えられる。

5. おわりに

本研究では、マイクロカプセルを用いた超音波DDS実現のため、体外からの超音波照射により分岐部を流れるカプセルの能動的流路選択の可能性について検討を行った。その結果、超音波の照射によって誘導される様子が観察された。そして流路分岐部にてカプセルを誘導するために必要な条件は、誘導する流路と超音波の進行方向が交差することである。今後は複雑な分岐部でもカプセルを誘導できる条件を数学的モデルによって確立することを目指す。

＜参考文献＞

(1) 橋田充：“ドラッグデリバリシステム－創薬と治療への新たなる挑戦－”、化学同人（1995）
(2) 石原謙：BME、Vol.6、No.1、pp.45-52（1992）
(3) 山田正敏・田畑泰彦：生体医工学、Vol.43、No.2、pp.238-246（2005）
(4) 工藤信樹・栗林香織・名取道也・森安史典・山本克之：電子情報通信学会論文誌A、Vol.J84A、No.12、pp.1492-1499（2001）
(5) 立花克郎：生体医工学、Vol.43、No.2、pp.211-215（2005）
(6) T.Makuta, F.Takemura：Physics of Fluids, Vol.18, No.10, 108102（2006）
(7) T.Lilliehorn, U.Simu, M.Nilsson, M.Almqvist, T.Stepinski, T.Laurell, J.Nilsson, and S.Johansson：Ultrasonics, Vol.43, No.5, pp.293-303（2005）
(8) Y.Yamakoshi and M.Koganezawa：Jpn. J. Appl. Phys., Vol.44, No.6B, 4583-4587（2005）
(9) 小塚晃透：日本音響学会誌、Vol.61、No.3、pp.154-159（2005）
(10) D.Koyama, A.Osaki, W.Kiyan and Y.Watanabe：IEEE Trans. Ultrason, Ferroelect. Freq. Contr., Vol.53, No.7, 1314-1321（2006）
(11) 工藤信樹・平尾紀文・岡田健吾・山本克之：電子情報通信学会和文誌、Vol.J89A、No.9、pp.746-753（2006）
(12) 桝田晃司・村松悠祐・瀋部一行・石原謙：生体医工学、Vol.46、No.2、pp.275-282（2008）
(13) Y.Muramatsu, S.Ueda, R.Nakamoto, Y.Nakayashiki, K.Masuda and K.Ishihara：Proc. of 4th European Medical & Biological Engineering Conference, pp.1589-1593（2008）
(14) K.Masuda, Y.Muramatsu, S.Ueda, R.Nakamoto, Y.Nakayashiki, and K.Ishihara：Jpn. J. Appl. Phys., Vol.48, No.7, 07GK03（2009）

【筆者紹介】

村松　悠佑
東京農工大学　大学院　生物システム応用科学府
生物システム応用科学専攻　博士前期課程修了
〒184-8588　東京都小金井市中町2-24-16
TEL：042-388-7130　FAX：042-388-7219

桝田　晃司
東京農工大学　大学院　生物システム応用科学府
准教授
〒184-8588　東京都小金井市中町2-24-16
TEL：042-388-7130　FAX：042-388-7219

32nd Annual International Conference of the IEEE EMBS
Buenos Aires, Argentina, August 31 - September 4, 2010

Study to prevent the Density of Microcapsules from diffusing in Blood Vessel by Local Acoustic Radiation Force

Kohji Masuda, *Member, IEEE*, Nobuyuki Watarai, Ryusuke Nakamoto, Yoshitaka Miyamoto, Keri Kim and Toshio Chiba

***Abstract*— We have already reported our attempt to constrain direction of microcapsules in flow owing to an acoustic radiation force. However, the diameter of capsules was too large not to be applied *in vivo*. Furthermore, acoustic radiation force affected only in focal area because focused ultrasound was used. Thus we have improved our experiment by using microcapsules as small as blood cells and introducing a plane wave of ultrasound. We prepared an artificial blood vessel including a Y-form bifurcation established two observation areas. Then we newly defined the induction index to evaluate the difference of capsule density in two paths of downstream. As the result, optimum angle of ultrasound emission to induce to desired path was derived. And the induction index increased in proportion to the central frequency of ultrasound, which is affected by forming aggregation of capsules to receive more radiation force.**

I. Introduction

MANY researches of drug delivery system (DDS) have been proposed by applying microcapsules or microbubbles as a drug carrier in human body [1-3]. The existence of capsules (or bubbles) improves the introduction efficiency to affect the target area by making use of sonoporation [4]. While the lifetime of the microbubbles is several minutes, we consider the microcapsules are better for use with various types of delivery. However, because of the diffusion of capsules after injection, it is difficult to deliver capsules from the point of injection to desired target area through bifurcations of blood vessel. If the behavior of capsules could be controlled and constrained the direction, the introduction efficiency would be enhanced. Owing to an acoustic radiation force [5-7], which is a physical phenomenon where an acoustic wave pushes an obstacle along its direction of propagation, we have ever reported our attempt to propel microcapsules in water [8,9]. We have elucidated the conditions in sound pressure, flow velocity and diameter of capsules for active path selection of capsules in an artificial blood vessel. However, because we used capsules which diameters were ranged more than 60 μm, so that they were too great to be applied *in vivo*. Furthermore, we also used focused ultrasound to concentrate acoustic radiation force, which affected only in focal area. Because an acoustic radiation force is proportional to the cube of the size of a capsule, larger acoustic field can produce more radiation force to propel a capsule in flow. Thus we have improved our experiment to adopt capsules as small as blood cells with a plane wave of ultrasound.

Considering micrometer-sized microcapsules, upon ultrasound exposure, they are oscillated to produce Bjerknes force and to aggregate each other [10] if the frequency of ultrasound is near their resonance frequency. We already confirmed aggregation of capsules in a straight flow when acoustic radiation force was produced in oncoming direction with MHz-order frequencies [8]. However, frequency dependence had not been elucidated when capsules were propelled in flow by the radiation force [11,12]. In this paper we investigated optimal condition to propel microcapsules in flow using plane wave of ultrasound with various frequencies.

II. Principle

Assuming that the shape of capsules is sphere and they are located in uniform acoustic field, an acoustic radiation force acts to propel a capsule in the direction of acoustic propagation. And when the microcapsules are placed in flow, a capsule should receive a flow resistance. If the acoustic radiation force is greater than the flow resistance, the trajectory of the capsule is curved, as shown in Fig.1.

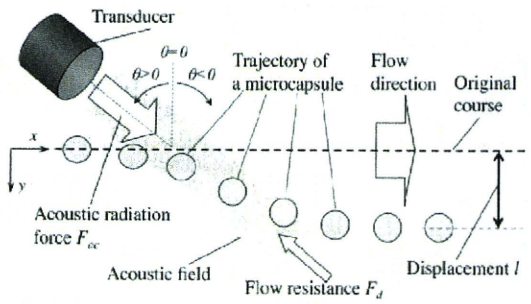

Fig.1. Trajectory of microcapsule in flow under ultrasound emission.

At a positive value of angle θ in Fig.1, a capsule is propelled to y-direction with lower flow resistance than at a negative value of angle θ. At larger absolute of angle θ, though a capsule passes through the acoustic field for a longer period, radiation force operates a capsule to propel in

Manuscript received April 1, 2010. This work was supported in part by Health Labor Sciences Research Grant 200813004A.

Kohji Masuda, Nobuyuki Watarai and Ryusuke Nakamoto are with Graduate School of Bio-Applications and Systems Engineering, Tokyo University of Agriculture and Technology, Koganei, Tokyo, 184-8588 Japan (e-mail: masuda_k@cc.tuat.ac.jp).

Yoshitaka Miyamoto is with School of Medicine, Nagoya University, Nagoya, 466-8550 Japan.

Keri Kim and Toshio Chiba is with National Center for Child Health and Development, Tokyo, 157-8535 Japan

978-1-4244-4124-2/10/$25.00 ©2010 IEEE

x-direction more than in y-direction. In Fig.1, although the shape of the acoustic field is expressed as a square, it is measured before the experiment. Here the acoustic radiation force is expressed as per the following equation [12,13]

$$F_{ac} = \pi r^2 Y_p P, \qquad (1)$$

where P is the mean energy density of the incident wave, Y_p is a dimensionless factor called radiation force function that depends on the scattering and absorption properties of the capsule and r is the radius of the capsule. Since Y_p does not include an item of frequency [14], it is valuable to investigate the effect of ultrasound frequency in F_{ac}.

III. Experiments

A. Diameter distribution of microcapsules

We used the F-04E microcapsule (Matsumoto Oil), which has a shell made of polyvinyl chloride (PVC), a specific gravity of 0.0225, and an average diameter of 4 μm. It contains isobutene inside and is stable in room temperature. We selected only those microcapsules with a diameter less than 5 μm by using micro sieves. We measured the diameter of more than 800 capsules through five microscope images to elucidate the diameter distribution of capsules. Figure 2 shows the diameter distribution of capsules as bars, where diameters of capsules between 2 and 3.5 μm are mostly included. Since the solid line in Fig.2 indicates the resonance frequency f of microbubble, which is calculated as per eq. (2) [6], the resonance frequency is ranged between 2 and 4 MHz according to the diameter.

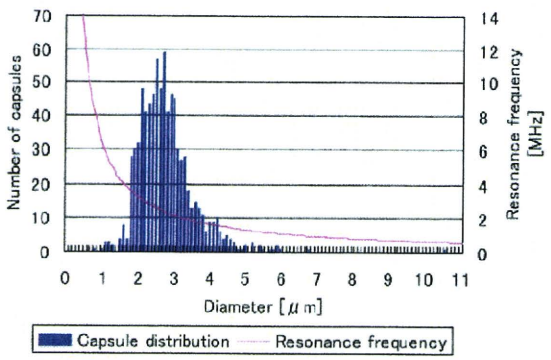

Fig. 2. The diameter distribution of F-04E microcapsules plotted with the resonance frequency of eq.(2) according to the diameter.

$$f = \frac{1}{2\pi r}\sqrt{\frac{3kP}{\rho}}, \qquad (2)$$

where k is the ratio of specific heats. However, because of the shell, the resonance frequency of microcapsules should be higher than that of microbubbles. According to a mathematical simulation [15], theoretical resonance frequency of microcapsules is estimated between 5 and 7 MHz with the diameter of 4 μm. Thus the behavior of capsules is considered to be mostly affected by MHz-order frequencies.

B. Observation of capsule behavior

We also have prepared an artificial blood vessel made of polyethylene glycol (PEG), including a Y-form bifurcation, as shown in the schematic view of Fig. 3. The external size was 85 x 55 x 10 mm^3 and inner diameter of the paths was 2 mm. The blood vessel was placed in the bottom of a water tank, which was filled with water. Because the acoustic impedance of PEG (sound velocity: 1540-1560 m/s, density: 1.27g/mL) is similar to that of water, the energy of ultrasound in water reaches the path with high efficiency. As shown in Fig.3, optical images of the observed areas 1 and 2 were recorded independently using a microscope (Omron, KH-7700) and an inverted microscope (Leica, DMRIB), respectively.

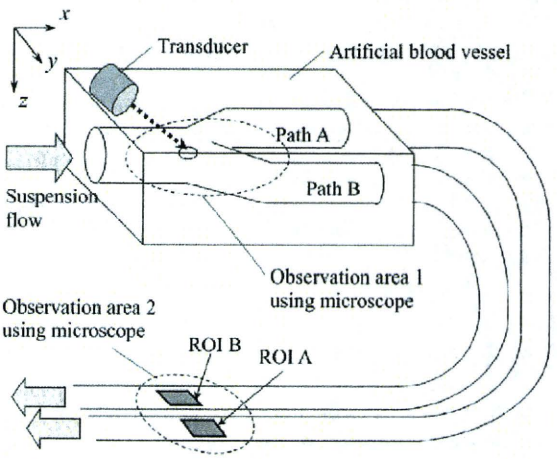

Fig.3. Schematic view of artificial blood vessel with the location of two observation areas.

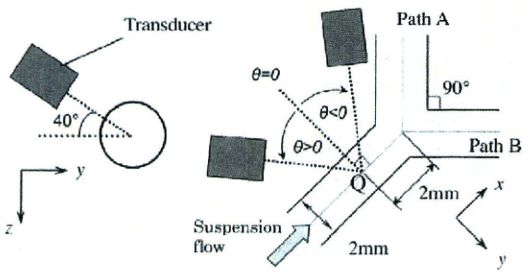

Fig.4. Position configuration between a transducer and the artificial blood vessel near the bifurcation.

Figure 4 shows the position configuration between a transducer and the artificial blood vessel near the bifurcation in the observed area 1. The axis of the transducer was set at 40 degrees from −y direction around the x-axis to prevent physical interference between the transducer and the edge of the water tank. The transducer included a flat ceramic disc with a diameter of 20 mm to emit plane wave of ultrasound. We have prepared five transducers, which have their center frequencies as 0.5, 1, 2, 3 and 5 MHz, respectively, to compare the effect between near and far from resonance frequencies. Measuring two-dimensional distribution of sound pressure in above five transducers, the half width of

ultrasound beam is ranged between 4 and 5 mm. Therefore the axis of the transducer was directed to the point Q, as shown in Fig. 4, which was set to be 2 mm from the bifurcation point to upstream course to adjust angle θ deg to the z-axis. The distance of the surface of a transducer from the point Q was set as between 50 and 60 mm so that the point Q is included in the area of highest sound pressure.

C. *Evaluation of induction of capsules to the desired path*

As shown in Fig.5, when ultrasound was emitted, aggregations of capsules were clearly observed to enter path B rather than A in the observation area 1, whereas neither aggregations of capsules nor significant difference between paths were observed without ultrasound. To evaluate the number of capsules that passed through each path, we extended the two paths using semitransparent tubes and established an observed area 2, where both paths were observable in a single view. Figure 6 shows microscope images of the observed area 2, which were captured using a high-speed camera (Casio, EX-F1) attached to the microscope with an interval time of 3.3 ms (300 fps), when capsule suspension was injected with flow velocity of 5 mm/s with ultrasound emission of 2 MHz and maximum sound pressure of 500 kPa. Because of the limitation of optical magnification, though individual microcapsules cannot be distinguished, thicker suspension was confirmed.

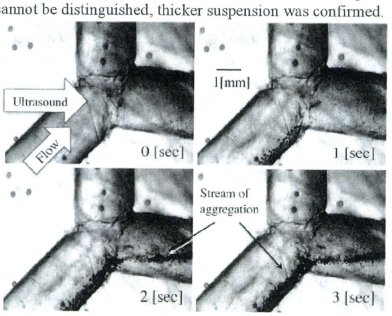

Fig.5.Transition of microscope images of observation area 1 after injection of capsule suspension (flow velocity: 20 mm/s, center frequency of ultrasound: 2 MHz and maximum sound pressure: 400 kPa).

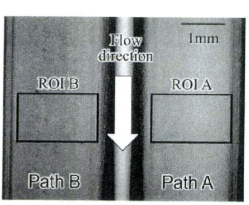

Fig.6. Microscope images of observation area 2, which was taken at 300 fps after injection of capsule suspension in flow velocity 5 mm/s with ultrasound emission of 2 MHz and maximum sound pressure as 500 kPa.

To measure amount of microcapsules, we established two square regions of interest (ROI), which size is 1.8 x 1.2 mm2, in each path (ROIs A and B) and calculated the average brightness. In the previous paper [8,9] we have evaluated amount of capsules by defining shadow index, which reflects brightness change according to existence of capsules in a ROI. However, the value of the shadow index cannot be compared between ROIs if there is initial brightness difference between them. Thus we newly defined the induction index by comparing two ROIs as follows.

Figure 7 shows variations of brightness average in both ROIs upon injection of a capsule suspension with flow velocity of 20 mm/s. Before the injection, brightness was constant but there was a difference between two ROIs. According to the appearance of capsules, after 7 s, brightness of both ROIs decreased simultaneously. A significant different variation was confirmed upon ultrasound emission of 2 MHz and 500 kPa, which indicates more capsules were induced to ROI B after 28 s. And according to disappearance of capsules, after 48 s, they returned to their initial brightness. Thus calculating the subtraction of brightness with capsules from initial brightness in each ROI, and comparing between ROIs, we have defined the induction index ξ_B of capsules to be induced to the path B rather than the path A using the following equation.

$$\xi_B = \frac{(I_B - I_{B0}) - (I_A - I_{A0})}{(I_B - I_{B0}) + (I_A - I_{A0})} \times 100 \ [\%], \quad (3)$$

where I_{A0} and I_{B0} indicate initial brightness average without capsules, and I_A and I_B indicate brightness average with capsules, in the ROI A and B, respectively. We confirmed that the induction index ξ_B reflects the relative ratio of capsules to pass ROI B versus total amount of capsules through our previously recorded movies [8,9] which calculated shadow index versus capsules density.

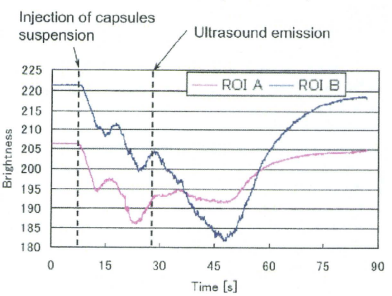

Fig.7. Variations of brightness average in ROIs A and B upon injection of a capsule suspension with flow velocity of 20 mm/s, before and after ultrasound emission of maximum sound pressure of 500 kPa and center frequency of 2 MHz.

IV. Results

Figure 8 shows the induction index ξ_B versus the angle of ultrasound emission θ for five kinds of maximum sound pressure, flow velocity of 20 mm/s and center frequency of 3 MHz. Here the value of induction index was calculated from the sampled frames recorded with high frame of 300 fps, while capsules were appeared in the frame under ultrasound emission. The number of sampled frames was set up to 300 frames, which depends on the duration of capsules appearance. When the sound pressure is less than 200 kPa, dominant induction to path B was observed in the positive angle of emission. When the sound pressure is more than 300 kPa, though capsule induction to path B was confirmed at angle of emission of -60 degree, significant induction to path B was confirmed at angle of emission of 30 degree. The optimum angle of ultrasound emission for induction to path B in the experiment was at an angle of 30 degree, which was used in the following experiment.

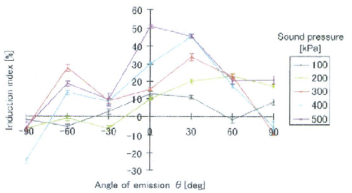

Fig.8. Induction index versus angle of emission with plane ultrasound of 3 MHz and flow velocity of 20 mm/s.

We measured the induction index upon emission of sinusoidal ultrasound with a frequency of 0.5, 1, 2, 3 and 5 MHz. Figure 9 shows the values of induction index versus the maximum sound pressure, where θ was fixed as 30 degree, when a flow velocity ranged as 20 mm/s. The induction index increased in proportion not only to the sound pressure but also to the central frequency of ultrasound. Regarding the central frequency, more capsules were induced to the desired path when it was close to the resonance frequency, which is supposed to be more than 5 MHz. We have considered that the result reflects the effect of aggregation of capsules.

Because capsules form aggregations under ultrasound emission, they should be equivalent to larger volume than isolated capsules. When the frequency is near resonance frequency, the capsules would be greatly oscillated to form larger aggregation and to receive more acoustic radiation force to the direction of propagation. We have to investigate behavior of capsules more precisely under various conditions of ultrasound.

From those results, using the higher pressure, higher frequency and plane ultrasound, the more capsules could be inducted to the desired path at the bifurcation of blood vessel. In the next step we are going to establish the behavior of capsules in flow theoretically before applying to *in vivo* experiment. The effect of acoustic streaming should be considered by using higher frequency than 5 MHz. Meanwhile we are going to develop a method to identify the precise location of bifurcations *in vivo* by detecting and constructing three-dimensional shape of the blood vessel.

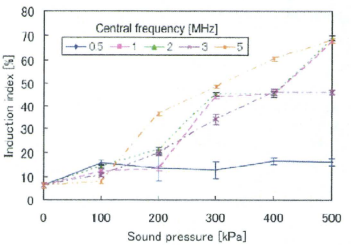

Fig.9. Induction index versus maximum sound pressure of plane ultrasound by the angle of emission of 30 deg in flow velocity of 20 mm/s.

V. Conclusions

In this study, we realized active control of microcapsules with a diameter less than 5 μm to constrain the direction in an artificial blood vessel. In a simple bifurcation, significant induction was confirmed when the angle of ultrasound emission was 30 degree from the rectangular of the flow to upstream. We confirmed that capsules were induced into the desired path using the higher pressure, higher frequency and plane ultrasound. For further analysis, the precise conditions necessary to realize active control of capsules in a complicated shape of blood vessel should be elucidated. Also we are going to consider applications for the future *in vivo* experiments.

References

[1] N.de Jong, R.Cornet, and C.T.Lancée: Ultrasonics 32 (1994) 447-453.
[2] K.Okada, N.Kudo, K.Niwa, and K.Yamamoto: J. Med. Ultrason. 32 (2005) 3-11.
[3] H.Zheng, P.Dayton, C.Caskey, S.Zhao, S.Qin, and K.Ferrara: Ultrasound in Med. & Biol., 33 (2007) 1978-1987.
[4] Y.Yamakoshi, Y. Koitabashi, N. Nakajima and T. Miwa: Jpn. J. Appl. Phys. 45 (2006) 4712-4717.
[5] J.J.Rychak, A.L.Klibanov, J.A.Hossack: IEEE Trans. Ultrason, Ferroelec. and Freq. Control, 52 (2005) 421-433.
[6] H.Mitome: Jpn. J. Appl. Phys. 40 (2001) 3484-3487.
[7] T. Kozuka, K. Yasui, T. Tuziuti, A. Towata, J. Lee, and Y. Iida: Jpn. J. Appl. Phys. 48 (2009) 07GM09.
[8] K.Masuda, R.Nakamoto, Y.Muramatsu, Y.Miyamoto, K.Kim and T. Chiba: Proc. of 31st Annual Intl Conf. IEEE EMBS (2009) 295-298.
[9] K.Masuda, Y.Muramatsu, S.Ueda, R.Nakamoto, Y.Nakayashiki, and K. Ishihara: Jpn. J. Appl. Phys. 48 (2009) 07GK03.
[10] Y. Yamakoshi and T. Miwa: Jpn. J. Appl. Phys. 47 (2008) 4127-4131.
[11] T. Lilliehorn, U. Simu, M. Nilsson, M. Almqvist, T. Stepinski, T. Laurell, J. Nilsson, and S. Johansson: Ultrasonics 43 (2005) 293-303.
[12] T.Hasegawa, Y.Hino, A.Annou, H.Noda, and M.Kato: J. Acoust. Soc. Am. 93 (1993) 154-161.
[13] F. G. Mitri: Wave motion 43 (2005) 12-19.
[14] T.Hasegawa, T.Kido, C.W.Min, T.Iizuka, and C.Matsuoka: Acoust. Sci. & Tech. 22 (2001) 273-281.
[15] K.Yasui, J.Lee, T.Tuziuti, A.Towata, T.Kozuka, and Y.Iida: J. Acoust. Soc. Am. 126 (2009) 973-982.

Ultrasound -Assisted Gene Transfer to Adipose Tissue-Derived Stem/Progenitor Cells (ASCs)

Yoshitaka Miyamoto[a, b], Hitomi Ueno[b], Rei Hokari[b], Wenji Yuan[b], Shuichi Kuno[b], Takashi Kakimoto[b], Shin Enosawa[c], Yoichi Negishi[d], Kiyoshi Yoshinaka[c], Yoichiro Matsumoto[e], Toshio Chiba[b], and Shuji Hayashi[a]

[a]*Department of Advanced Medicine in Biotechnology and Robotics, Nagoya University Graduate School of Medicine, Higashi-ku, Nagoya 461-0047, Japan.*
[b]*Department of Clinical Research & Development, National Center for Child Health and Development, Tokyo, Japan.*
[c]*Department of Innovative Surgery, National Research Institute for Child Health and Development, Tokyo, Japan.*
[d]*Department of Drug and Gene Delivery System, School of Pharmacy, Tokyo University of Pharmacy and Life Science, Hachioji, Tokyo, Japan.*
[e]*Department of Mechanical Engineering, The University of Tokyo, Tokyo, Japan.*

Abstract. In recent years, multilineage adipose tissue-derived stem cells (ASCs) have become increasingly attractive as a promising source for cell transplantation and regenerative medicine. Particular interest has been expressed in the potential to make tissue stem cells, such as ASCs and marrow stromal cells (MSCs), differentiate by gene transfection. Gene transfection using highly efficient viral vectors such as adeno- and sendai viruses have been developed for this purpose. Sonoporation, or ultrasound (US)-assisted gene transfer, is an alternative gene manipulation technique which employs the creation of a jet stream by ultrasonic microbubble cavitation. Sonoporation using non-viral vectors is expected to be a much safer, although less efficient, tool for prospective clinical gene therapy. In this report, we assessed the efficacy of the sonoporation technique for gene transfer to ASCs. We isolated and cultured adipocyets from mouse adipose tissue. ASCs that have the potential to differentiate with transformation into adipocytes or osteoblasts were obtained. Using the US-assisted system, plasmid DNA containing beta-galactosidase (beta-Gal) and green fluorescent protein (GFP) genes were transferred to the ASCs. For this purpose, a Sonopore 4000 (NEPAGENE Co.) and a Sonazoid (Daiichi Sankyo Co.) instrument were used in combination. ASCs were subjected to US (3.1 MHz, 50% duty cycle, burst rate 2.0 Hz, intensity 1.2 W/cm^2, exposure time 30 sec). We observed that the gene was more efficiently transferred with increased concentrations of plasmid DNA (5-150 μg/mL). However, further optimization of the US parameters is required, as the gene transfer efficiency was still relatively low. In conclusion, we herein demonstrate that a gene can be transferred to ASCs using our US-assisted system. In regenerative medicine, this system might resolve the current issues surrounding the use of viral vectors for gene transfer.

Keywords: adipose tissue-derived stem/progenitor cells (ASCs), adipo/osteogenic potential, sonoporation, microbubble, gene transfer.
PACS: 87.18.Ed, 87.17.Uv, 87.18.Hf, 92.40.vu, 87.14.Df

INTRODUCTION

In recent years, multilineage adipose tissue-derived stem cells (ASCs) have become increasingly attractive as a promising source for cell transplantation and regenerative medicine [1-2]. Particular interest has been expressed with regard to the possibility that stem cells, such as ASCs and marrow stromal cells (MSCs), can be made to differentiate into a number of different cell or tissue types by means of gene transfer. Gene transfection using highly efficient viral vectors [3], such as adeno- and sendai viruses, have been adopted for this purpose. Sonoporation, a form of ultrasound (US)-assisted gene transfer, is an alternative gene manipulation technique which employs the creation of a jet stream by ultrasonic microbubble cavitation [4-5]. Sonoporation using non-viral vectors is expected to be a much safer, although less efficient, tool for prospective clinical gene therapy. In this study, we assessed the efficacy of the sonoporation technique for gene transfer to ASCs.

ISOLATION AND CULTURE OF ASCs

Subcutaneous adipose tissue was obtained from 8 week old adult mice (CLEA Japan, Inc. Meguro, Tokyo, Japan). A 0.5g specimen of adipose tissue was washed three times with Hank's balanced salt solution, cut finely, and digested with 1 ml of 1 mg/ml type I collagenase (Collagenase Type I, 274U/mg, Koken Co., Ltd., Tokyo, Japan) for 45 min in a 37°C water bath with reciprocal shaking. Cells obtained after filtering the digested tissue through 100μm meshes were suspended in Dulbecco's modified Eagle's medium (DMEM)/F12 containing 20% fetal bovine serum and centrifuged at 1,200 rpm for 5 min at room temperature, then the sedimentary cell layer was collected. Suspension and centrifugation of the sedimentary cells was repeated three times before the cells were plated in culture flasks.

For attached culture, 1×10^5 adipocytes (sedimentary cells) were seeded into a T-25 flask (NUNC) with DMEM/F12 containing 20% FBS, 100 U/ml penicillin and 100 μg/ml streptomycin at 37°C in a humidified atmosphere of 5% CO_2. After the cells attached and spread, they were passaged. This growth/passaging cycle was repeated twice.

Mouse ASCs were successfully cultured, forming confluent monolayers (FIGURE 1.a). The cells had both adipogenic (FIGURE 1.b, [6]) and osteogenic differentiation capabilities (FIGURE 1.c). These data suggest that the harvested cells included adipose tissue-derived stem cells.

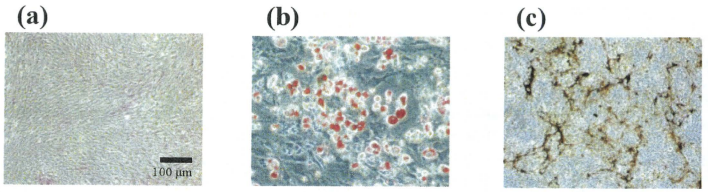

FIGURE 1. Adipo/osteogenic differentiation of ASCs. (a) The morphology of isolated and cultured ASCs. (b) Adipogenic differentiation of ASCs. The cells were stained with Oil Red O 1 week after adipogenic induction. (c) Osteogenic differentiation of ASCs. The cells were stained with Von Kossa stain 1 week after osteogenic induction. Scale bar, 100 μm.

US-ASSISTED GENE TRANSFER USING DIFFERENT METHODS

A total of 2×10^4 cells per well were grown in 96-well microplates. Following mixing of the microbubbles/DNA, the microplates were then subjected to ultrasound (frequency 3.1 MHz, duty cycle 50%, burst rate 2.0 Hz, intensity 1.27 W/cm^2, exposure time 30 sec) using a Sonopore 4000 (8 mm diameter probe; Nepa Gene Co. Ltd., Chiba, Japan). The CMV-LacZ cDNA plasmid was obtained from Clontech (Palo Alto, CA). DNA was used at a concentration of 20 μg/ml, and for transfer to the ASCs, 20μg/900μl of plasmid was mixed with a 100 μl volume of the sonazoid microbubbles (Daiichi Sankyo Corporation, Tokyo, Japan) to achieve a final concentration of 10% microbubbles.

Two methods were used for US exposure during the gene transfer tests (FIGURE 2). The first subjected the cells to the ultrasound on their attaching side (FIGURE 2, Method-1). For the second method, cells were subjected to ultrasound from the other side (FIGURE 2, Method-2). The microbubbles float on top as time passes. Therefore, compared to Method-1, the Method-2 approach results in a longer contact of microbubbles with the cells.

After the cells were transduced with the gene using ultrasound, they were incubated for 24 h and then assessed for their Lac Z gene expression. LacZ expression in the cells was detected by the X-gal staining method. The beta-galactosidase activity in the cells was detected as a method for evaluating gene transfer, thereby allowing for the easy identification of the cells expressing the Lac Z gene (X-Gal Staining Assay Kit (A10300K); Genlantis).

Although the samples showed no staining without sonazoid and/or US (FIGURE 3.a), they were positively stained when both 10% sonazoid and US were used (FIGURE 3.b and c). When Method-1 was used, the gene transfer efficiency was improved by reducing the amount (100-30μl) of the preparation solution in each well. Because the distance between the microbubbles and the attached cells is small, Method-1 is subject to sonoporation as well as Method-2. Therefore, we adopted

Method-1 because the experimental technique is simple and effective. The figure below shows both methods of gene transfer (FIGURE 2).

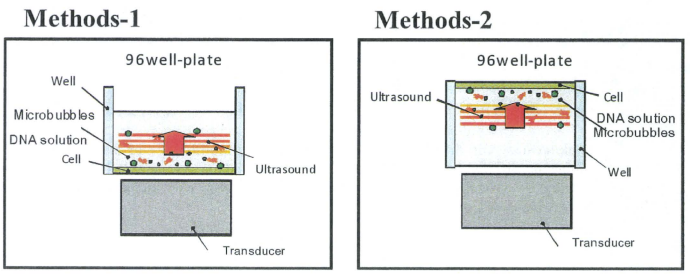

FIGURE 2. Two methods were used for US exposure. Methods-1: cells were subjected to ultrasound on the attaching side. Methods-2: cells were exposed to ultrasound from the other, non-attached, side.

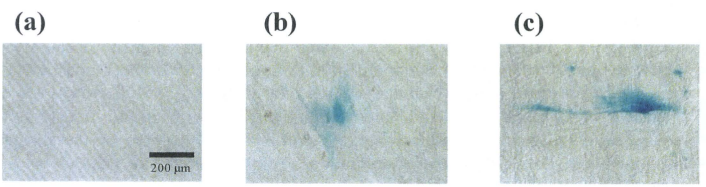

FIGURE 3. Microscopy after CMV-LacZ cDNA plasmid gene transfer. (a) Light microscopy of a normal control sample (with the Luc Z gene) without sonoporation. (b) Light microscopy revealed Luc Z expression after sonoporation with Luc Z genes and sonazoid using Methods-1. (c) Light microscopy revealed Luc Z expression after sonoporation with the Luc Z genes and sonazoid using Methods-2. Scale bar, 200 μm.

THE EFFECTS OF THE MICROBUBBLES

The cells (2×10^4 per well) were subjected to US (frequency 3.1 MHz, duty cycle 50%, burst rate 2.0 Hz, intensity 1.27 W/cm^2, exposure time 30 sec). We observed that the gene was more efficiently transferred with increased concentrations of sonazoid (0-40%). The effect of the microbubbles (sonazoid), and its effect on cell viability and cellular damage were analyzed by MTT assay using a Cell Counting Kit-8 (CCK-8; DOJINDO LABORATORIES, Kumamoto, Japan). Briefly, the CCK-8 reagent (10 μL) was added to each well and the reaction was allowed to occur for up to 2 hr. The absorption of the sample at 450 nm was measured against a background control, using a microplate reader. The cell number was counted after sonoporation.

The cell viability of ASCs before and after sonoporation was examined using a Cell Counting Kit-8 (FIGURE 4). After sonoporation with 10% sonazoid, the ASCs showed a lower viability compared to control ASCs and ASCs after sonoporation with 20-40% sonazoid. However, the cells most efficiently transferred the gene when the sonazoid concentration was 10% (data not shown). This confirmed that the ultrasonic microbubble cavitation occurred efficiently, therefore we then examined the impact of the concentrations of the GFP gene on the gene transfer efficiency.

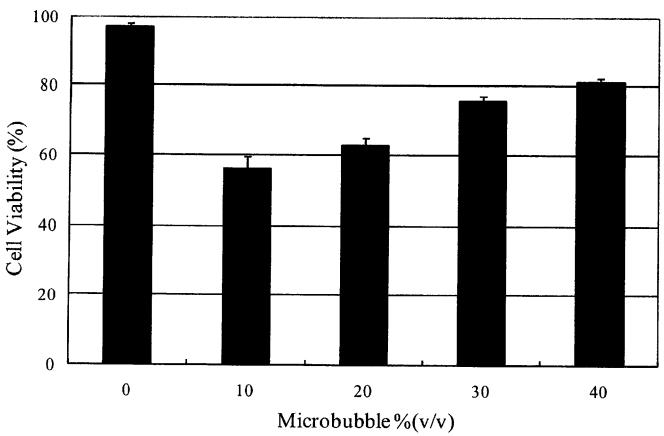

FIGURE 4. The viability of ASCs before/after sonoporation (0-40%). In these experiments, 2×10^4 cells per well were subjected to US (frequency 3.1 MHz, duty cycle 50%, burst rate 2.0 Hz, intensity 1.27 W/cm^2) for 30 sec.

US-ASSISTED GENE TRANSFER IN VITRO

In this series of experiments, 2×10^4 cells per well were subjected to US (frequency: 3.1 MHz, duty cycle: 50%, burst rate 2.0 Hz, intensity: 1.27 W/cm^2) for 30 sec. A green fluorescent protein (GFP)-encoding plasmid, pEGFP-N3, was obtained from Clontech (Palo Alto, CA). ASCs sonoporated with and without 10% sonazoid showed GFP expression after 24h by fluorescence microscopy (FIGURE 5).

Although the samples showed no expression of GFP when the ultrasound was applied without sonazoid (FIGURE 5.b, pEGFP-N3: 60 μg/ml), they did express GFP when both 10% sonazoid and US were used (FIGURE 5.c, pEGFP-N3: 60 μg/ml). The gene was more efficiently transferred with increased concentrations of the GFP gene (5-150 μg/ml, data not shown).

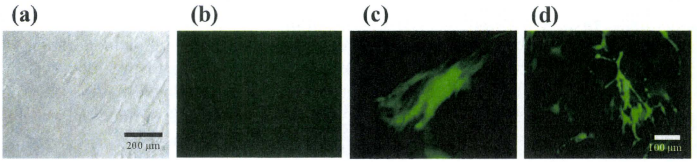

FIGURE 5. Microscopy after GFP gene transfer. (a) Light microscopy of a normal control sample without sonoporation and GFP gene transfer (60 μg/ml). (b) Fluorescent microscopy of a normal control sample without GFP expression. (c, d) Fluorescent microscopy revealed GFP expression after sonoporation with the GFP gene (60 μg/ml) and 10% sonazoid. Scale bar, 100-200 μm.

CONCLUSIONS

This study assessed the gene transfer efficiency of sonoporation in mouse ASCs. Although approximately 40% of the cells were no longer viable after sonoporation, gene transfer to the remaining cells was observed. However, the efficiency of gene transfer was relatively low. It is therefore necessary to improve gene transfer conditions (ultrasound conditions, microbubbles, DNA concentration, etc) in order to improve the gene transfer efficiency of this procedure.

ACKNOWLEDGMENTS

We thank Ms. Rina Yokota (Nagoya University) for her valuable assistance. This work was supported in part by Health and Labor Sciences Research Grants from the Ministry of Health, Labor and Welfare (Tokyo, Japan).

REFERENCES

1. J. M. Gimble, A. J. Katz, and B. A. Bunnell, *Circ Res.* **100(9)**, 1249-1260 (2007).
2. Y. Miyamoto, K. Oishi, H. Yukawa, H. Noguchi, M. Sasaki, H. Iwata and S. Hayashi, *Cell Transplant.* accept.
3. H. Yukawa, H. Noguchi, K. Oishi, M. Inoue, M. Hasegawa, M. Hamaguchi, N. Hamajima and S. Hayashi, *Cell Transplant.* **18(5)**, 601-609 (2009).
4. K. Tachibana, *Hum Cell.* **17(1)**, 7-15 (2004).
5. D. L. Miller, M. A. Averkiou, A. A. Brayman, E. C. Everbach, C. K. Holland, J. H. Wible Jr and J. Wu, *J Ultrasound Med.* **27(4)**, 611-632 (2008).
6. M. Ono, Y. Aratani, I. Kitagawa and Y. Kitagawa, *Exp. Cell Res.* **187**, 309–314 (1990).

Cell Transplantation, Vol. 19, pp. 701–706, 2010
Printed in the USA.

0963-6897/10 $90.00 + .00
DOI: 10.3727/096368910X508799
E-ISSN 1555-3892
www.cognizantcommunication.com

An Improvement in the Attaching Capability of Cryopreserved Human Hepatocytes by a Proteinaceous High Molecule, Sericin, in the Serum-Free Solution

Yoshitaka Miyamoto,*[1] Naozumi Teramoto,† Shuji Hayashi,‡ and Shin Enosawa*

*Clinical Research Center, National Center for Child Health and Development, Tokyo, Japan
†Department of Life and Environmental Sciences, Faculty of Engineering, Chiba Institute of Technology, Chiba, Japan
‡Department of Advanced Medicine in Biotechnology and Robotics, Nagoya University Graduate School of Medicine, Nagoya, Japan

The methodology of cryopreservation of human hepatocytes remains unsatisfactory. Even when the viability of thawed cells is tolerable, the cells often lose the attaching capability to a culture dish, resulting in the cells' inability to survive. Previously, we described the effectiveness of maltose on the attachment of hepatocytes. This article demonstrates that a silk-derived high molecular protein, sericin, improves the cell-attaching capability in the serum-free freezing medium. When human hepatocytes [initial viability: 60.9 ± 3.1% (mean ± SD, $n = 3$)] were frozen with serum-free Dulbecco's modified Eagle medium (DMEM) containing 10% dimethyl sulfoxide (DMSO), the viability was 29.4 ± 3.2% and the cell-attaching capability 20.4 ± 4.1%. On the other hand, DMEM containing 10% DMSO and 1% sericin increased the values to 45.0 ± 0.8% and 26.2 ± 3.2%. Moreover, the addition of 0.1 mol/L maltose to the sericin-containing medium improved to 42.2 ± 3.2% and 51.1 ± 1.0%, as we demonstrated in a previous report. The present results indicated that sericin combined with maltose is a novel additive in the serum-free freezing medium for human hepatocytes.

Key words: Cryopreservation; Human hepatocytes; Sericin

INTRODUCTION

An improvement in the cryopreservation of hepatocytes is expected to greatly benefit not only the research field but also the clinical cell transplantation field. The present major requirement is that pharmaceutical companies use human hepatocytes for predicting the metabolism of drug candidates (2). The potential demand will be elevated in clinical cell transplantation and the bioartificial liver. The number of cases of hepatocyte transplantation is gradually increasing, and in some cases the cells were transplanted repeatedly from the same donor to confirm effectiveness (5). Consequently, a reliable cryopreservation protocol needs to be established. However, hepatocytes easily lose their cell viability after cryopreservation.

We noticed that the cell viability immediately after thawing does not reflect the cells' survival in the culture condition. Therefore, we have been trying to improve cell survival by a modification of the freezing medium. Previously, we reported the different efficacies of oligosaccharides on the attachment capability of cryopreserved hepatocytes and arrived at the conclusion that maltose is the most effective additive (6), while trehalose, which belongs to the same dissaccharide as maltose, is thought to be effective elsewhere (3,4). Therefore, we embarked on the development of a serum-free freezing solution to ensure the safety of cells for clinical transplantation, especially to avoid xenozoonoses.

Sericin is a silk-derived high molecular protein and was reported recently to be useful for cell cryopreservation (7), but the effectiveness for cryopreservation of primary hepatocytes has not been tested. Here we demonstrate that sericin can replace serum in the freezing solution, and that the addition of maltose resulted in a marked improvement in the cell-attaching capability after thawing.

MATERIALS AND METHODS

Materials

The materials used in the present study were obtained as follows. Dulbecco's modified Eagle medium (DMEM),

Received June 1, 2009; final acceptance April 21, 2010. Online prepub date: June 3, 2010.
[1]Present address: Department of Advanced Medicine in Biotechnology and Robotics, Nagoya University Graduate School of Medicine, Nagoya 466-8550, Japan.
Address correspondence to Shin Enosawa, Clinical Research Center, National Center for Child Health and Development, 2-10-1 Ookura, Setagaya-ku, Tokyo 157-8535, Japan. Tel: +81-3-3416-0181; Fax: +81-3-3417-2864; E-mail: senosawa@nch.go.jp

Williams medium E, and antibiotics (penicillin, streptomycin, and kanamycin) were from GIBCO BRL, Life Technologies (Grand Island, NY). Fetal bovine serum (FBS) was produced from Gemini Bio-Products (West Sacramento, CA). Insulin, dexamethasone, and dimethyl sulfoxide (DMSO, D-2650) were purchased from Sigma-Aldrich (St. Louis, MO). Maltose was obtained from Wako Pure Chemical Industries, Ltd. (Osaka, Japan). A Live/Dead Viability Cytotoxicity Kit (L3224) was obtained from Molecular Probes (Eugene, OR). All other materials and chemicals not specified above were of the highest grade. Sericin hydrolysate with an average molecular mass of 30 kDa was generously supplied from Seiren Co. Ltd. (Fukui, Japan).

Procurement of Human Primary Hepatocytes

Human hepatocytes were isolated from the nontransplantable livers of three different donors (age/race/sex/cold ischemia time: 34/African-American/female/38 h; 36/Caucasian/male/30 h; 57/Asian/male/27 h) originally procured by the National Disease Research Interchange (NDRI) in Philadelphia (USA), and imported by the Human and Animal Bridging Research (HAB) Organization (Chiba, Japan). The cell isolation was performed by a collagenase perfusion method as described previously (6).

Hepatocyte Freezing and Thawing Procedures

The basic composition of the cryopreservation medium was DMEM containing 100 U/ml penicillin, 100 U/ml streptomycin, and 10% DMSO. Maltose was added to this medium at concentrations of 0.1 mol/L and sericin at 1%. One milliliter of cell suspension containing 5×10^6 cells was quickly transferred to a 2.0-ml freezing tube and placed in a controlled rate freezer (Kryo10, Planer, Middlesex, UK). The freezing protocol was described previously (6). Immediately after freezing, the tubes were transferred to liquid nitrogen and stored for 1–3 months. In order to thaw cells, the tubes were placed in a 37°C water bath for 90 s. The cell suspension was then diluted one- to ninefold with ice-cold DMEM. The suspension was centrifuged for 1 min at $50 \times g$. After the supernatant was removed, the cells were resuspended in fresh medium and the cell viability was assessed by a trypan blue exclusion test. The final concentration of trypan blue (GIBCO BRL) was 0.2%.

Hepatocyte Culture and Determination of Cell Survival

Freshly isolated or cryopreserved/thawed hepatocytes (4×10^5 live cells) were seeded into 35-mm collagen-coated dishes (Biocoat Cellware, Bedford, MA) in 2 ml of Williams medium E containing 10% FBS, 1 μmol/L insulin, 1 μmol/l dexamethasone, 100 μg/ml kanamycin, 100 U/ml penicillin, and 100 U/ml streptomycin. The cells were incubated at 37°C under a humidified 5% CO_2 atmosphere. The culture medium was changed at 6 and 24 h after seeding. The cell survival rates were estimated by microscopic observation of the attached cells 24 h after seeding, using the NIH IMAGE program (National Institutes of Health, http://rsb.info.nih.gov/nih-image/). Two fields in each well of three wells (total six fields) were examined and the average was calculated. In order to confirm the viability of cultured cells, hepatocytes were stained with calcein and ethidium bromide (Live/Dead Viability/Cytotoxicity Kit).

Osmolality Measurements and Differential Scanning Calorimetry (DSC) Analysis

The osmolality of freezing medium was measured using a Vapor Pressure Osmometer (VAPRO 5520, Wescor, USA). Differential scanning calorimetry (DSC) was performed by a Perkin Elmer differential scanning calorimeter, Diamond DSC, under a helium atmosphere using a cooling attachment with liquid nitrogen. For the measurement, 5 μl of the sample was taken into a small aluminum pan. The temperature of the sample was changed according to the same programmed schedule as was used for the hepatocyte cryopreservation.

Ethical Consideration

All experimental procedures using human hepatocytes were performed after permission from the institutional review board of National Center for Child Health and Development.

RESULTS

Survival of Human Hepatocytes Cryopreserved Under Different Conditions

The representative microscopic appearances of the cultured hepatocytes from a 34-year-old African-American female are shown in Figure 1. Almost all attached cells had transparent cytoplasm with a firm smooth surface. Because the culture medium was aspirated and plated, washed extensively, and supplied with fresh medium at 6 h after inoculation, there were few dead cells attached to the plate except for small-sized round nuclei. In fact, when cells were stained with calcein and ethidium bromide, all cells are calsein-positive live cells and only the small, probably naked nuclei were stained red by ethidium bromide (Fig. 1K). It was apparent that the cells cryopreserved in DMEM-containing DMSO and maltose (Fig. 1D), and containing DMSO, maltose, and sericin (Fig. 1G) attached well onto the culture plate and that these cells had a better appearance than that of the freshly isolated hepatocytes (Fig. 1A). The attachment of cells stored in DMEM-containing DMSO and sericin (Fig. 1E) was slightly better than the attachment of the cells stored in DMEM containing DMSO only (Fig. 1B), containing DMSO and FBS (Fig. 1C), and containing

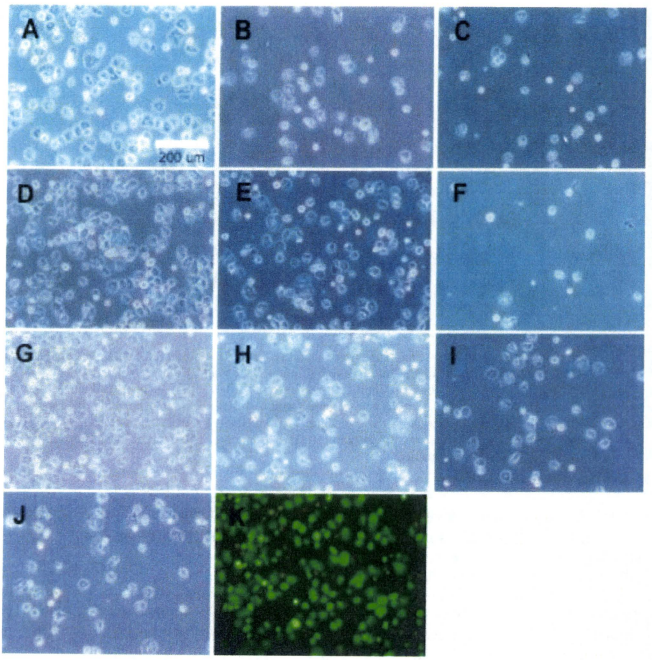

Figure 1. The phase-contrast photomicrographs of human hepatocytes before (A) and after the cryopreservation (B–G). The hepatocytes were cultured on type I collagen cell culture dish for 24 h after the inoculation. Scale bar: 200 μm. The hepatocytes were cryopreserved with DMEM containing 10% DMSO (base medium) (B), base medium + 10% FBS (C), base medium + 0.1 mol/L maltose (D), base medium + 1% sericin (E), base medium + 10% FBS, 1% sericin (F), base medium + 0.1 mol/L maltose, 1% sericin (G), base medium + 10% FBS, 0.1 mol/L maltose (H), base medium + 10%FBS, 0.1mol/L maltose, 1% sericin (I), Cell Banker 1 (J). (K) Fluorescent photomicrograph of (G) after staining with calcein and ethidium.

DMSO, FBS, and maltose (Fig. 1H). In contrast, the combination of FBS and sericin did not appear favorable for the cryopreservation (Fig. 1F, I). The cell attachment after storage by a commercially available cryopreservant, Cell Banker 1 (Fig. 1J) was the same as that for DMEM-containing DMSO and FBS (Fig. 1B).

Quantitative Evaluation of Cell Viability and Cell-Attaching Capability

In order to quantify the morphological differences, we determined the cell viability immediately after thawing and the cell-attaching capability (Fig. 2A and B, respectively). The values of the two indices are of independent nature, one from numbers of viable and total cells and the other from an occupied area in the microscopic field. The initial viability of freshly isolated hepatocytes was 61 ± 3.1% (condition 1, average ± SD, n = 3). The viability of cells cryopreserved in DMEM-containing DMSO only was 29 ± 3.2% and cell attachment was 20.4 ± 4.1%. When we used the other control, Cell Banker 1, the cell viability was reasonably good (46.0 ± 1.1%), but the cell attachment capability was quite low (13.4 ± 1.5%). This type of discrepancy between the initial cell viability and cell survival was often observed with the cryopreserved hepatocytes. The addition of FBS did not improve the cell viability (condition 3, 30.2 ±

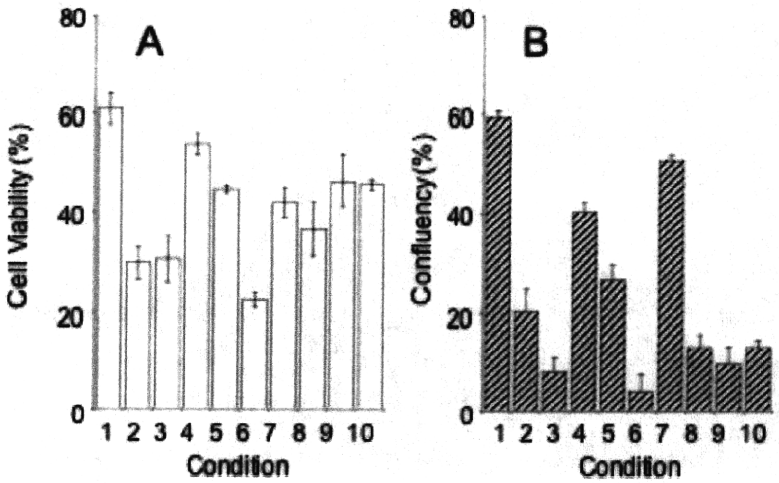

Figure 2. Cell viability (A) and attaching capability (B) of cryopreserved human hepatocytes with a different composition of the preservation solution. 1: Freshly isolated hepatocytes; 2: DMEM containing 10% DMSO (base medium); 3: base medium + 10% FBS; 4: base medium + 0.1 mol/L maltose; 5: base medium + 1% sericin; 6: base medium + 10% FBS, 1% sericin; 7: base medium + 0.1 mol/L maltose, 1% sericin; 8: base medium + 10% FBS, 0.1 mol/L maltose; 9: base medium + 10% FBS, 0.1 mol/L maltose, 1% sericin; 10: Cell Banker 1. The data are the means and SD of three independent experiments.

4.7%), but maltose (condition 4, viability: 54.0 ± 2.1%, attaching capability: 40.2 ± 2.2%) and sericin (condition 5, viability: 45.0 ± 0.8%, attaching capability: 26.2 ± 3.2%) increased both the cell viability and attaching capability. The most marked effect was observed with DMEM-containing DMSO, maltose, and sericin (condition 7, viability: 42.2 ± 3.2%, attaching capability: 51.0 ± 1.0%). As expected from the morphological observation (Fig. 1), the combination of sericin and FBS decreased both the cell viability and attaching capability (condition 6), while the addition of maltose resulted in more favorable values for the corresponding controls (conditions 8 and 9).

Comparison of Physical Characteristics of Freezing Solutions

The osmolality of the freezing solution is listed in Table 1. The value of DMEM culture medium was 0.312 mol/kg, almost equal to that of typical isotonic solutions (0.28–0.29 mol/kg, data not shown). When DMSO was added, the value increased to 1.922 but no marked elevation occurred by the addition of FBS, maltose, or sericin. Figure 3 shows the DSC analysis of the effect of maltose and sericin in the freezing solution. The spike indicates the starting point of crystallization. Each additive affected the crystallization temperature. Interestingly, the solution containing both sericin and maltose showed crystallization at the earlier phases containing sericin or maltose only. However, no obvious relationships were observed between the cell biological protecting activity and the physical parameters this time.

DISCUSSION

A lot of factors have been proposed to cause cell damage by cryopreservation, such as ice crystal formation, condensation of salts the free water, dehydration, etc. (8). After laborious efforts by numerous researchers, DMSO has emerged as one of the major cryoprotective agent for cells. However, DMSO itself does not sufficiently protect the cell from damage during the cryopreservation process. We previously reported that the addition of maltose to DMSO-based serum containing cryopreservation medium improved the cell-attaching capability of hepatocytes (6). In this report, we demon-

Table 1. Osmolality of Various Freezing Media Used for Human Hepatocytes

Composition	Osmolality (mol/kg)
1. DMEM only	0.312
2. DMEM, 10% DMSO	1.922
3. DMEM, 10% DMSO, 10% FBS	1.965
4. DMEM, 10% DMSO, 0.1 mol/L maltose	1.943
5. DMEM, 10% DMSO, 1% sericin	1.963
6. DMEM, 10% DMSO, 0.1 mol/L maltose, 1% sericin	1.978

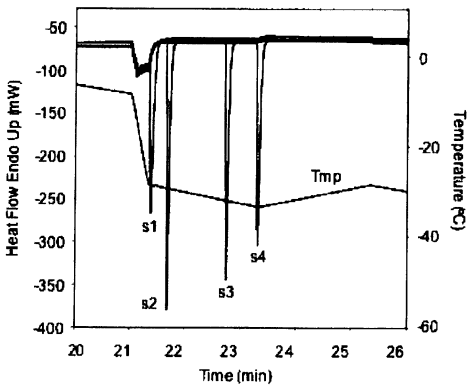

Figure 3. The effect of the additives in the freezing media by differential scanning calorimetry (DSC) analysis. s(spike)1: DMEM containing 10% DMSO (base medium); s2: base medium + 0.1 mol/L maltose, 1% sericin; s3: base medium + 1% sericin; s4: base medium + 0.1 mol/L maltose. Tmp indicates the temperature of the test medium. The solution temperature of each spike: s1: −28.0°C, s2: −29.1°C, s3: −31.8°C, s4: −32.5°C.

strated that silk origin protein, sericin, can replace serum in the medium.

The advantage of serum-free medium is not merely the avoidance of xenozoonoses, but the emergence of quality differences of the serum lots. Sericin is a protein hydrolysate from raw silk and it is rich in serine (an average molecular weight of 30 kDa). Recently, sericin was reported as a novel cryopreservation agent of mammalian and insect cell lines (7). We expanded the utility of sericin to primary hepatocytes, cells that are perhaps the most difficult to storevia freezing. Because of the advantages described above, sericin-containing medium may become one option for the clinical transplantation of cryopreserved hepatocytes.

Ice crystal formation is likely to be a major hurdle to succeed cryopreservation. DSC measurement is often used to study ice formation in the multicomponent liquid phase (1). Unfortunately, no meaningful relationship between cell biological assessment and DSC as well as osmolality was gleaned from the present results, but the diligence of these physical approaches should be conducted in conjunction with biological evaluations.

ACKNOWLEDGMENTS: Firstly, we would like to express deep gratitude to the persons who donated the livers for research and to their family members. We also thank Dr. Satoshi Suzuki of HAB Research Organization, Japan for supplying the human hepatocytes and Seiren Co. Ltd., Fukui, Japan for the generous gift of sericin. This research was supported by Grant-in-aid (KH71066 and KHD1027) from the Japan Health Sciences Foundation, Tokyo, Japan and by the Sasakawa Scientific Research Grant from The Japan Science Society.

REFERENCES

1. Bryant, G. DSC measurement of cell suspensions during successive freezing runs: Implications for the mechanisms of intracellular ice formation. Cryobiology 32:114–128; 1995.
2. Hewitt, N. J.; Lech, M. J.; Houston, J. B.; Hallifax, D.; Brown, H. S.; Maurel, P.; Kenna, J. G.; Gustavsson, L.; Lohmann, C.; Skonberg, C.; Guillouzo, A.; Tuschl, G.; Li, A. P.; LeCluyse, E.; Groothuis, G. M.; Hengstler, J. G. Primary hepatocytes: current understanding of the regulation of metabolic enzymes and transporter proteins, and pharmaceutical practice for the use of hepatocytes in metabolism, enzyme induction, transporter, clearance, and hepatotoxicity studies. Drug Metab. Rev. 39:159–234; 2007.
3. Illouz, S.; Nakamura, T.; Webb, M.; Thava, B.; Bikchandani, J.; Robertson, G.; Lloyd, D.; Berry, D.; Wada, H.; Dennison, A. Comparison of University of Wisconsin and ET-Kyoto preservation solutions for the cryopreservation of primary human hepatocytes. Transplant. Proc. 40:1706–1709; 2008.
4. Katenz, E.; Vondran, F. W.; Schwartlander, R.; Pless, G.; Gong, X.; Cheng, X.; Neuhaus, P.; Sauer, I. M. Cryopreservation of primary human hepatocytes: the benefit of trehalose as an additional cryoprotective agent. Liver Transpl. 13:38–45; 2007.
5. Lee, K. W.; Lee, J. H.; Shin, S. W.; Kim, S. J.; Joh, J. W.; Lee, D. H.; Kim, J. W.; Park, H. Y.; Lee, S. Y.; Lee,

H. H.; Park, J. W.; Kim, S. Y.; Yoon, H. H.; Jung, D. H.; Choe, Y. H.; Lee, S. K. Hepatocyte transplantation for glycogen storage disease type Ib. Cell Transplant. 16:629–637; 2007.
6. Miyamoto, Y.; Suzuki, S.; Nomura, K.; Enosawa, S. Improvement of hepatocyte viability after cryopreservation by supplementation of long-chain oligosaccharide in the freezing medium in rats and humans. Cell Transplant. 15:911–919; 2006.
7. Sasaki, M.; Kato, Y.; Yamada, H.; Terada, S. Development of a novel serum-free freezing medium for mammalian cells using the silk protein sericin. Biotechnol. Appl. Biochem. 42:183–188; 2005.
8. Terry, C.; Dhawan, A.; Mitry, R. R.; Hughes, R. D. Cryopreservation of isolated human hepatocytes for transplantation: State of the art. Cryobiology 53:149–159; 2006.